Arch. Metall. Mater. **70** (2025), 4, 1955-1964

DOI: https://doi.org/10.24425/amm.2025.156282

S. QIAN[1,2*], H. LI[1], J.-H. CAO[1], Z.-Q. MA[1], D.-X. GUO[1]

PREDICTION MODEL FOR C-WARPING DEFECT OF STEEL STRIP IN CONTINUOUS ANNEALING PROCESS OF HOT-DIP GALVANIZING

The C-warping of steel strip in the continuous annealing process (CAP) of hot-dip galvanizing unit (HGU) increases the risk of strip defects and uneven coating, which lead to the poor quality of strip products. Considering the process and the equipment characteristics of CAP, the forming mechanism of C-warping defect was analysed in detail by plastoelasticity theory. Subsequently, the C-warping mechanical model was deduced and the strip element method was applied to establish C-warping prediction model. And then, the optimization recursion method was used to solve the problem that C-warping defect was difficult to be forecasted. Finally, workflow of the C-warping prediction was formulated and applied on site. The model was used to forecast the strip shape of five typical specifications strip in different processes of the continuous annealing furnace (CAF) of Line 108 and 208. Analysis results show that the deviation between the predicted and measured values of the unit outlet strip shape can meet the requirements of product precision. The model can predict the strip shape of each process in CAF for real time and provide theoretical guidance for the subsequent process parameter optimisation. Thus, the model has the value of further popularisation and application.

Keywords: CAP of HGU; uneven coating; prediction model of C-warping defects; optimization recursion method; strip shape evolution of steel strip

1. Introduction

In recent years, with the rapid development of modern smart household, new energy vehicles, photovoltaic electrical equipment and other emerging industries, hot-dip galvanized strip has been widely used because of its low price and excellent corrosion resistance. At same time, customers have set forth higher requirements for the surface coating quality of steel strip. The quality of coating on the strip surface depends on strip shape of CAF outlet substrate. However, the transverse warping of the strip, referred to as C-warping defect, often happens during CAP, which is not only affecting its overall appearance but also causing the uneven coating, thereby reducing the quality grade and yield of the product [1]. When the strip with C-warping defect passes through the air knife gap, it leads to the large difference in the transverse distribution of the pressure or impulse acting on the strip surface from the air knife jet flow. So the coating thickness distribution of the strip surface is also difference. Under the large warping strip scraping zinc, the scraping phenomenon will happen, which makes the strip difficultly pass through the gap between two air knife and more seriously lead to strip breakage.

Previous studies on C-warping mainly focus on hot rolling, cold rolling and temper-rolling processes. For the C-warping defect in the hot temper-rolling processes, the defect mechanism was analysed, and the process parameters were optimized to reduce the degree of C-warping [2,3]. In view of the cold and temper-rolling processes, some typical scholars, such as Zhang, used finite element method to analyse the mechanism, deformation law and shape evolution of common flatness defects in temper-rolling and cold rolling [4,5]. Qin transformed the three-dimensional elastic problem of C-warping into plane problem and established C-warping finite element model by using spline finite element method [6]. Zhang et al. proposed the mechanical deformation mechanism through mechanical modelling and simulation calculation for the complex plate warping defects of cold rolled extremely thin plate and discussed the warping deformation law and influencing factors [7]. Tang et al. analysed warping cause and proposed the control strategy during continuous annealing, temper-rolling and secondary cold rolling [8-10]. MASUI et al. studied the generation mechanism and influence law of C-warping in the annealing furnace [11]. However, throughout these studies, the research on the C-warping problem

[1] HUANGSHAN UNIVERSITY, COLLEGE OF MECHANICAL AND ELECTRICAL ENGINEERING, HUANGSHAN, ANHUI, 245041 CHINA
[2] YANSHAN UNIVERSITY, NATIONAL ENGINEERING TECHNOLOGY RESEARCH CENTER FOR EQUIPMENT AND TECHNOLOGY OF COLD STRIP ROLLING, QINHUANGDAO, HEBEI, 066004 CHINA

* Corresponding author: nds12121@163.com

in the annealing process of hot-dip galvanizing and prediction for C-warping defect is rarely reported in the literatures. It is still difficult but a focus of technical research on site that the formation mechanism of C-warping strip is analysed, and the prediction technology of C-warping strip is developed. In this context, this paper conducts relevant research on these problems.

2. Analysis on the formation mechanism of C-warping strip

HGU consists of two parts, namely, CAP and hot-dip galvanizing process (HGP). CAP is divided into five processes, preparatory heating section (PHS), direct fire section (DFS), radiant heating section (RHS), cooling section (CS), and tension direct roller section (TDRS), as shown in Fig. 1. Considering that TDRS is short and compensates the CS temperature, it is combined with CS.

Firstly, the strip are preheated about 200°C in PHS. In DFS, rolling oil of the strip surface are burned directly by open flame burners and the surface temperature is rapidly increasing. In RHS, the strip is heated to the recrystallisation temperature range (700°C-900°C) for a period. In CS, the high-speed protective gas from slot nozzles with symmetrically arranged in the furnace is sprayed to the strip surface so that the strip temperature is controlled within hot-dip temperature range. And then, the strip entering the zinc pot and go through the sinking roller system, the final coating is obtained by gas knife scraping zinc [12-13].

2.1. Formation mechanism of C-warping defect

In the high temperature of the furnace, the mechanical properties of the material, such as elastic modulus and yield strength, change nonlinearly with temperature increasing. So the relationship between elastic modulus (EM) and temperature, the relationship between yield strength (YS) and temperature are characterized by elastic modulus reduction coefficient (EMRC) χ_T and yield strength reduction coefficient (YSRC) η_T, respectively. EMRC and YSRC decrease nonlinearly with the temperature increasing, as shown in Fig. 2. As the temperature

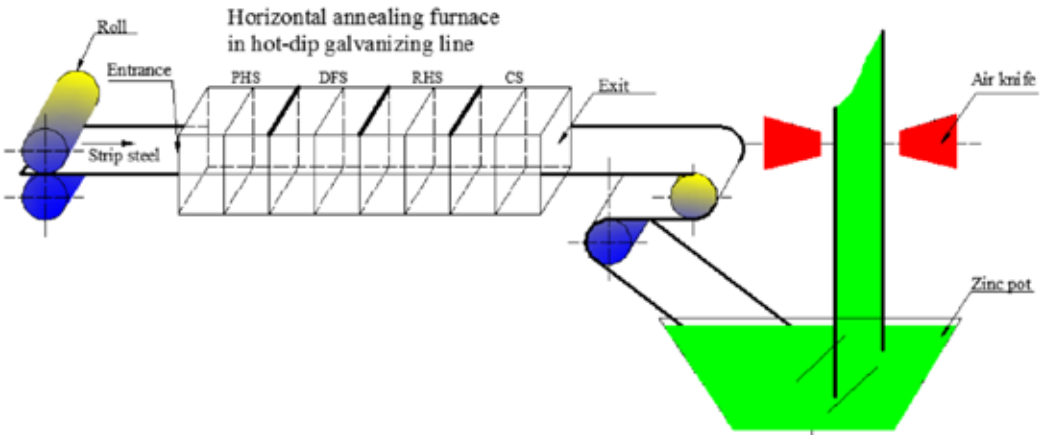

Fig. 1. Composition of HGU

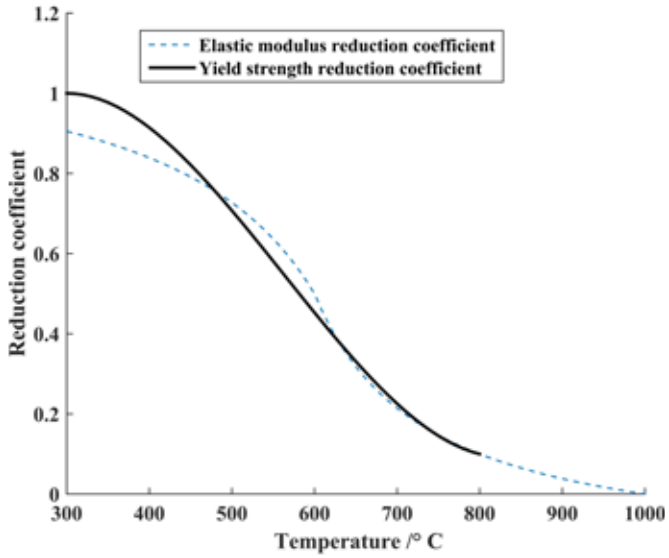

Fig. 2. EMRC and YSRC evolving with temperature

rises, the material plasticity increased gradually. When the temperature is close to 700°C-900°C, the strip loses bearing capacity and the material plasticity is large [14].

The non-uniform temperature of the strip causes the thermal expansion degree vary greatly. Considering the boundary that the tension in the strip and the mutual constraints of the strip structure result in thermal stress inside the plate, there must be thermal deformation. Combined with Fig. 2, it is found that the plasticity of the material is enhanced when the strip temperature rises to about 770°C-790°C. The figure also shows that the yield strength and elastic modulus of the strip are about 0.2 times of those at room temperature [14]. In this condition, if the thermal stress exceeds the yield strength, then the strip easily transformed to plastic deformation from elastic deformation. The plastic deformation of the strip is divided into two parts: transverse plastic deformation (referred to as deformation A) and thick plastic deformation (referred to as deformation B). Deformation B

can be ignored because the thickness of the strip is relatively small. In the case of asymmetric heating in the furnace, if the upper surface temperature of the strip is less than the lower surface temperature, then deformation A is unevenly distributed along the thickness direction under the action of thermal stress, as shown in Fig. 3(a). When the strip passes through CS, the cooling fan sprays the cooling gas on the strip surface, and the strip temperature drops to about 560℃-620℃. Within this temperature range, the yield strength and elastic modulus of the strip increase, but the plastic deformation of the strip does not occur easily. Deformation A, which has been generated during heating, is again transformed into the transverse stress of the strip, as shown in Fig. 3(b). When the internal stress of the strip exceeds the critical stability condition, the strip will be unstable, and its appearance is C-warping defect, as shown in Fig. 3(c).

In CAF, due to the limitations of the heating device, the surface temperature of the strip are differences in transverse, thick and longitudinal directions, which causes greatly different for the thermal expansion degree in short time. Considering that the strip subjected to tension and its inner mutual constraints result in thermal stress inside the plate, there must be thermal deformation. When the thermal stress exceeds YS, then the strip easily transformed to plastic deformation from elastic deformation. In addition, the mechanical properties of the strip decrease with the temperature increasing, and then there is uneven transverse plastic deformation in the thickness direction of the strip. As the strip temperature decreases, the residual thermal stress exceeds the instability condition and warping deformation occurs.

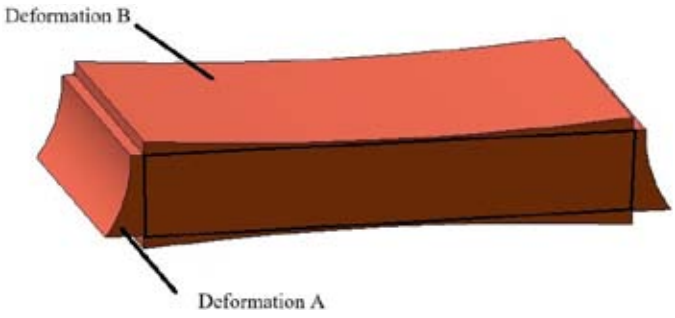

Fig. 3(a). Plate shape of the strip steel during heating

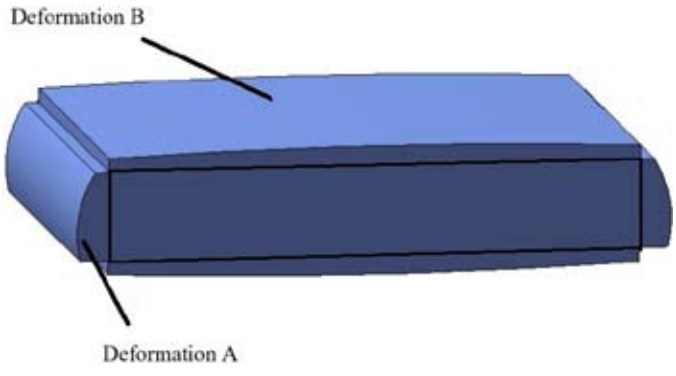

Fig. 3(b). Plate shape of the strip steel during cooling

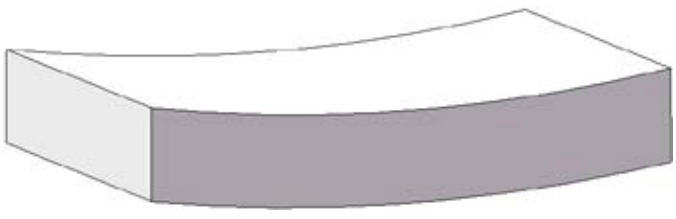

Fig. 3(c). Plate shape warping of the strip steel after instability

2.2. Establishment of C-warping defect mechanical model

To describe the degree of C-warping quantitatively, a section steel strip with length L_0 between two adjacent furnace rollers is selected for analysis. As shown in Fig. 4, a rectangular coordinate system, the width midpoint of strip neutral layer as the origin, is established. The x direction is the strip longitudinal direction, and the y direction is the strip transverse direction. The C-warping is a warping deformation of z direction, and the amount of warping is expressed by the z direction displacement w. It stipulated that the strip shows upper C-warping when $w > 0$ and the strip shows lower C-warping when $w < 0$.

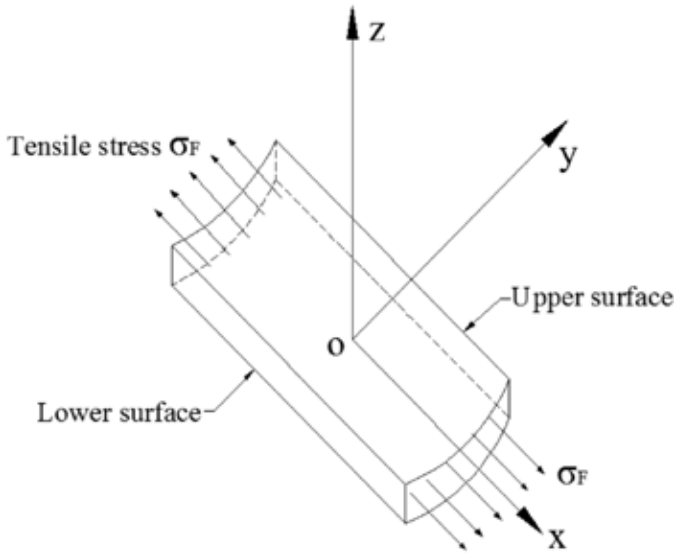

Fig. 4. Force analysis of strip

Although the strip warping deformation includes elastic deformation and plastic deformation, the elastic deformation will be restored under the strip temperature is uniform or normal temperature, and the final warping deformation of the strip is produced in the plastic deformation stage. Therefore, the C-warping mechanical model is established by elastoplastic theory. The maximum internal force contributing to C-warping deformation is temperature-dependent equivalent bending moment M_T and y direction positive force N_y. However, contact area between the strip and the furnace roller is small and there is no relative sliding, so N_y can be ignored [15]. According to the basic equation of thermoelasticity theory of the thin plate, the differential equation of thin plate bending can be derived by Eq. (1) [16].

$$\begin{cases} D\nabla^2\nabla^2 w = -\nabla^2 M_T \\ D = \int_{-H/2}^{H/2} \dfrac{z^2 E}{1-\mu^2} dz \\ M_T = \dfrac{E\alpha}{1-\mu} \int_{-H/2}^{H/2} Tz dz \end{cases} \tag{1}$$

where D is the bending stiffness of the plate (N.mm^{-1}), M_T is temperature-dependent equivalent bending moment (N.mm^{-1}), E is elastic modulus of the plate at room temperature (MPa); α is thermal expansion coefficient of the plate (°C^{-1}), μ is Poisson ratio, H is thickness of the strip (mm), and T is temperature distribution on the strip surface (°C), ∇^2 is Laplacian, $\nabla^2 = \dfrac{\partial^2}{\partial x^2} + \dfrac{\partial^2}{\partial y^2}$, $\nabla^2\nabla^2 = \dfrac{\partial^4}{\partial x^4} + 2\dfrac{\partial^4}{\partial x^2 \partial y^2} + \dfrac{\partial^4}{\partial y^4}$.

Assuming that the strip neutral layer displacement is independent of x and the strip plastic strain is linearly distributed along the thickness direction [15]. The plastic strain is set as the initial strain. Three-dimensional initial normal strain and initial shear strain can be expressed by Eq. (2).

$$\begin{cases} \varepsilon_x^0 = \varepsilon_z^0 = 0 \\ \varepsilon_y^0(y,z) = \dfrac{\varepsilon_B}{H} z \\ \gamma_{xy}^0 = \gamma_{yz}^0 = \gamma_{xz}^0 = 0 \end{cases} \tag{2}$$

where ε_x^0, ε_y^0, ε_z^0 are the initial normal strain along x direction, y direction and z direction respectively, γ_{xy}^0 is initial shear strain of y plane in normal x direction, γ_{yz}^0 is initial shear strain of z plane in normal y direction, γ_{xz}^0 is initial shear strain of z plane in normal x direction, ε_B is the maximum transverse plastic strain difference of the strip. According to the geometrical, equilibrium and physical equations of the plate thermoelastic mechanics, Eq. (2) is substituted by the Eq. (1) and then relevant calculations are made. The amount of warping in the midpoint of the strip is selected as zero, and the curvature is zero. The boundaries of the section strip is simplified into simply supported at both ends along x direction and free at both ends along y direction. C-warping defect mechanical model (CDMM) can be established by Eq. (3)

$$\begin{cases} u = 0 \\ v = \dfrac{\varepsilon_B}{H} yz \\ w = -\dfrac{1}{2}\dfrac{\varepsilon_B}{H} y^2 \end{cases} \tag{3}$$

where u is the strip displacement along x direction, and v is the strip displacement along y direction.

The maximum transverse plastic strain difference ε_B is determined by the maximum value of the transverse plastic strain ε_p in a cross section. Any cross section of the strip undergo the same temperature change, so arbitrary cross section at $x = x_0$ of the strip is obtained and its temperature distribution function $T = T(x_0, y, z)$ is considered. Therefore, the plastic strain ε_p of this cross section is established, and then the maximum plastic strain difference ε_B of this cross section is calculated from Eq. (4).

$$\begin{cases} \Delta T = T(x_0, y, z) - T_0(x_0, y, z) \\ \varepsilon_p = h(x_0, y, z) = \bar{\alpha}\Delta T - \left(\eta_T \sigma_s / \chi_T E + \psi\mu\sigma_F / \chi_T E\right) \\ \varepsilon_B = h_{\max}(x_0, y, z) - h_{\min}(x_0, y, z) \end{cases} \tag{4}$$

where ΔT is the temperature difference on the strip surface at cross section $x = x_0$, $T_0(x_0, y, z)$ and $T(x_0, y, z)$ are the temperature distribution at the beginning and end of periods τ in the cross section at $x = x_0$, $h(x_0, y, z)$ is the plastic strain function in the cross section at $x = x_0$, $\bar{\alpha}$ is the average thermal expansion coefficient in the cross section of strip $x = x_0$, η_T is YSRC at the temperature $T(x_0, y, z)$ of the cross section at $x = x_0$, χ_T is EMRC at the temperature $T(x_0, y, z)$ of the cross section at $x = x_0$, σ_s is YS of the strip at nomal temperature, ψ is temperature correlation coefficient, $\psi = -1$ when heating and $\psi = 1$ when cooling, $\varepsilon_p = h(x, y, z)$ is the plastic strain function, $h_{\max}(x_0, y, z)$ and $h_{\min}(x_0, y, z)$ are the maximum value and minimum value of plastic strain function $h(x_0, y, z)$ in the cross section of the strip at $x = x_0$, respectively.

3. Establishment of strip C-warping prediction model

In actual production, CAF is closed and therefore, it is necessary to predict the shape of each process section in the furnace combined with the process parameters of the unit and C-warping prediction model of the strip can provide support for the online tracking and adjustment of the actual production.

However, the surface temperature of the strip is different along three directions in CAP, and the temperature difference is not constant at all places, which making ε_p different at all places. This makes CDMM difficult to be applied in engineering. Therefore, a numerical calculation method, namely, strip element method, is used to establish strip C-warping prediction model based on CDMM.

3.1. C-warping prediction model realized by strip element method

The section strip with length L_0 between two adjacent furnace rolls is evenly divided into $2k + 1$ transverse strip elements along the x direction and evenly divided into $2n + 1$ layers in the z direction (Fig. 5). The width of each strip element is $\Delta x = L_0/(2k + 1)$, and the thickness of each strip element is $\Delta z = H/(2n + 1)$.

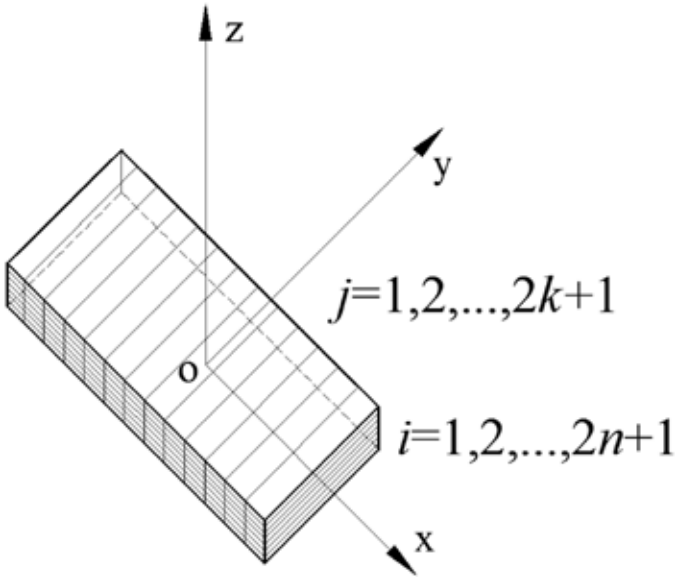

Fig. 5. Strip divided into transverse strip elements

The strip elements are treated as $(2n + 1)\times(2k + 1)$ array. Row elements of the array are strip element arranged along x direction, and column elements of the array are strip element arranged along z direction. The initial temperature distribution of any element is T_{ij}. Considering that Δx and Δz are very small, T_{ij} can be considered as the function about y. If the strip element is processed for a time τ in CAF, the temperature is T'_{ij}. Therefore, the thermal strain of the strip element ε_{ij} in row i and column j can be expressed as

$$\varepsilon_{ij} = \alpha_{ij}(T'_{ij} - T_{ij}) = \varepsilon_{emij} + \varepsilon_{pij} + \psi\mu\varepsilon_{Fij} \tag{5}$$

where i is the row subscript, j is the column subscript, α_{ij} is the average thermal expansion coefficient of each element, ε_{emij} is the maximum elastic strain of the strip element in row i and column j, ε_{pij} is the plastic strain of the strip element in row i and column j, and ε_{Fij} is transverse strain of the strip element in row i and column j under longitudinal tension. Eq. (5) is changed to a form that represents the plastic strain ε_{pij} of the strip element in row i and column j. The form of the plastic strain ε_{pij} is given by Eq. (6).

$$\varepsilon_{p_{ij}} = \alpha_{ij}(T'_{ij} - T_{ij}) - \frac{\eta_{Tij}\sigma_s}{\chi_{Tij}E} - \psi\mu\frac{\sigma_F}{\chi_{Tij}E} \tag{6}$$

where η_{Tij} is YSRC of the strip element in row i and column j under temperature distribution T_{ij}, χ_{Tij} is EMRC of the strip element in row i and column j under temperature distribution T_{ij}, and σ_F is the tensile stress of the strip under longitudinal tension. Each column strip elements are represented by vectors as follows

$$\mathbf{b_j} = \mathbf{a_j}^T(\mathbf{t'_j} - \mathbf{t_j}) - \frac{\sigma_s}{E}\mathbf{c_j} - \psi\mu\mathbf{d_j} \tag{7}$$

where, vectors $\mathbf{a_j}$, $\mathbf{b_j}$, $\mathbf{t_j}$, $\mathbf{t'_j}$, $\mathbf{c_j}$, $\mathbf{d_j}$ are all $2n + 1$ dimensional column vectors, $\mathbf{a_j} = (\alpha_{ij})_{(2n+1)\times 1}$, $\mathbf{a_j}^T$ is the transposed row vector of $\mathbf{a_j}$, $\mathbf{a_j}^T = (\alpha_{ij})_{1\times(2n+1)}$, $\mathbf{b_j} = (\varepsilon_{pij})_{(2n+1)\times 1}$, $\mathbf{t_j} = (T_{ij})_{(2n+1)\times 1}$, $\mathbf{t'_j} = (T'_{ij})_{(2n+1)\times 1}$, $\mathbf{c_j} = (\eta_{Tij}/\chi_{Tij})_{(2n+1)\times 1}$, $\mathbf{d_j} = (\varepsilon_{Fij})_{(2n+1)\times 1}$.

The maximum and minimum values of plastic strain $(\varepsilon_{p_{ij}})_{\max}$ and $(\varepsilon_{p_{ij}})_{\min}$ are determined in each column in the plastic strain vector $\mathbf{b_j}$. Thus, the maximum plastic strain difference ε_{Bj} is determined in each strip element.

$$\varepsilon_{Bj} = \left(\varepsilon_{p_{ij}}\right)_{\max} - \left(\varepsilon_{p_{ij}}\right)_{\min} \tag{8}$$

Then, for the strip with width B, the arbitrary points of the transverse strip elements can be represented by coordinate range $-B/2 \le y \le B/2$. According to Eq. (4), the warping distribution of the transverse strip elements of any column can be determined as

$$w_j = -\frac{1}{2}\frac{\varepsilon_{Bj}}{H}y^2 \qquad j = 1, 2, \cdots, 2k+1 \tag{9}$$

3.2. Acquisition strip shape of each process section in CAP

In order to grasp the warping degree of the strip in real time and adjust the process parameters to improve the outlet strip shape, it is necessary to predict the strip shape of each process section in CAP. It is found from the site that there are many factors affecting the strip shape, and the strip temperature is the main factor affecting its C-warping. However, under the actual working conditions, only the temperature of individual points in the middle of the strip can be obtained, and the strip surface temperature distribution along transverse direction cannot be obtained. Therefore, the strip shape in CAF is obtained by optimization recursive method.

The outlet strip shape of HGU can be obtained by measuring the surface coating of the strip, and the warp can be expressed in vector form $\mathbf{W^g}$

$$\mathbf{W^g} = \left(w_1^g, w_2^g, ..., w_j^g, ..., w_{(2k+1)}^g\right) \tag{10}$$

Optimization recursive method is used to solve the problem based on the outlet strip shape of the unit in order to obtain the shape of each process section in the furnace. Firstly, the strip shape of the downstream process section (the process section closing to the outlet of the unit) in the furnace is solved by the optimization recursive method based on the outlet strip shape of the unit. For the upstream process section (the process section closing to the inlet of the unit), it is calculated again by this method according to the strip shape of downstream process section. The steps of the optimization recursive method are performed as follows:

1) Setting of strip warping distribution for the section in CAF
Firstly, the set value of strip warping distribution in a process section of CAP can be expressed by vector $\mathbf{W}_f$ as

$$\mathbf{W}_f = (w_{f1}, w_{f2}, ..., w_{fj}, ..., w_{f(2k+1)}) \tag{11}$$

where f is the subscript of the strip warping distribution in each process section, namely, number of each process sec-

tion in furnace. For PHS, DFS, RHS and CS, f = 1,2,3,4, respectively.

2) Establishing temperature distribution vector $\mathbf{T}_f$ and $\Delta\mathbf{T}_f$

$$\begin{cases} T_{fj}^{s} = T_0^{s} + \dfrac{4\Delta T_h^{s}}{B^2} y^2 \\ T_{fj}^{x} = T_0^{x} + \Delta T_c + \dfrac{4\Delta T_h^{x}}{B^2} y^2 \\ T_{1j} = T_{fj}^{s}, T_{2k+1,j} = T_{fj}^{x} \\ \rho c \dfrac{V}{L}\left(T'_{ij} - T_{ij}\right) = \lambda \dfrac{2T_{ij} - T_{i,j-1} - T_{i,j+1}}{(\Delta x)^2} + \\ \qquad + \lambda \dfrac{2T_{ij} - T_{i+1,j} - T_{i-1,j}}{(\Delta z)^2} \\ \mathbf{T}_f = \left(T_{f1}, T_{f2}, ..., T_{fj}, ..., T_{f(2k+1)}\right) \end{cases} \tag{12}$$

3) Setting recursive quantity of strip warping distribution and optimization recursive

For a downstream process section of CAP, $\Delta\mathbf{W}_f$ is its recursive quantity. The set value of the warping distribution of the process section is continuously increased by recursive quantity and the theoretical value of the strip warping distribution at the outlet $\mathbf{W^b}$ is obtained.

$$\begin{cases} \Delta\mathbf{W}_f = h'(\mathbf{T}_f, \Delta\mathbf{T}_f) \\ \mathbf{W^b} = \mathbf{W}_f + \lambda\Delta\mathbf{W}_f \\ \mathbf{W^b} = \left(w_1^b, w_2^b, ..., w_j^b, ..., w_{(2k+1)}^b\right) \\ \lambda \le \lambda_{\max} \end{cases} \tag{12}$$

where, $\mathbf{T}_f$ is the temperature distribution vector of upper and lower surfaces of the strip in a process section, $\Delta\mathbf{T}_f$ is the temperature increment vector of upper and lower surface of the strip in a process section, λ is adjustment factor of the optimization recursive method, $h'(\mathbf{T}_f, \Delta\mathbf{T}_f)$ is a vector function with variables $\mathbf{T}_f$ and $\Delta\mathbf{T}_f$, w_j^b is the theoretical value of the warping distribution of the j row transverse strip element in CAP, $\lambda_{\max}$ is the allowable maximum value of adjustment factor of the optimization recursive method.

Optimization recursive objective function is established on the basis of least square method, and expressed by Eq. (13)

$$\begin{cases} \varphi(\mathbf{W^b}) = \sum_{i=1}^{2k+1}\left[\dfrac{w_j^b - w_j^g}{w_j^g}\right]^2 \\ \varphi_{\min}(\mathbf{W^b}) \le \psi^* \end{cases} \tag{13}$$

where ψ^* is maximum relative deviation between theoretical value and actual value of strip warping. The values of λ and $\Delta\mathbf{T}_f$ are changed to minimize the objective function $\phi(\mathbf{W^b})$ for determining the prediction value of the strip warping distribution of a downstream process section in CAP.

Based on the strip C-warping prediction model and the optimization recursive method, the prediction process of strip C-warping for CAP is compiled. As shown in Fig. 6, a theoretical basis is provides to quickly and accurately grasp evolution process of the strip shape in each process section of the unit.

4. On-site application of strip C-warping defect prediction model

In order to monitor the uniformity of the zinc coating on the strip steel and the impact of temperature on shape defects in CAF of a HGU, as well as to track the shape of the strip during

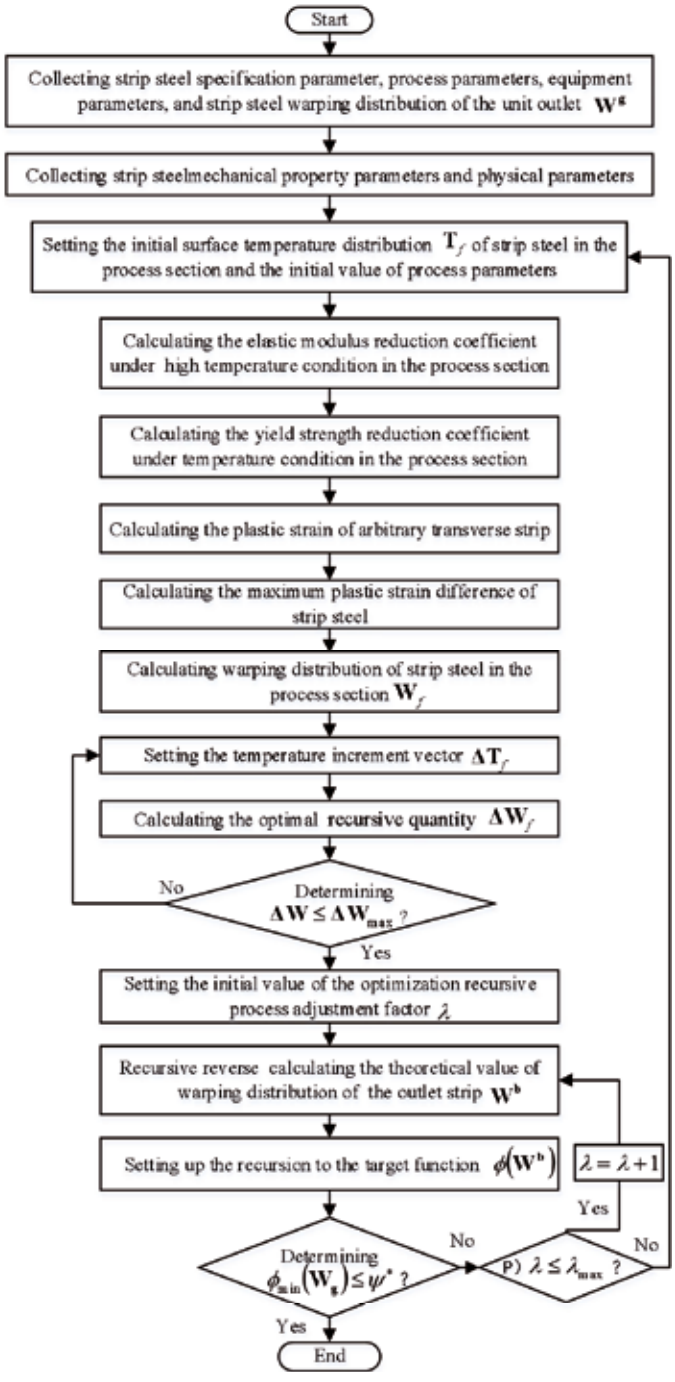

Fig. 6. Flow chart of prediction C-warping for strip

its operation in the furnace and at the exit, a model for predicting C-warping of the strip during CAP has been developed. This model is tailored to the characteristics of the equipment and production process of the line. The C-warping prediction process shows that subsequent segment deformation patterns are generally consistent with those of previous segments. Therefore, for computational convenience, the C-warping distribution of the strip steel is described using the warping distribution within any selected 1-meter length.

To validate the calculation accuracy of the prediction model, we focused on three significant specifications of strip steel produced in the Line 208, namely, specification I (1250 mm×2 mm, steel grade DC51D+AZ), specification II (1000 mm×0.5 mm, steel grade S350GD+AZ), and specification III (1000 mm×0.6 mm, steel grade S550GD+AZ). Additionally, we selected two widely produced specifications of the Line 108: specification IV (1200 mm×0.5 mm, steel grade DC51D+AZ) and specification V (1000 mm×0.37 mm, steel grade S300GD+AZ). The predicted values for the warping at the unit outlet were compared with the actual measured values, as illustrated in Fig. 7 to Fig. 11.

Furthermore, we calculated the relative errors between the maximum predicted C-warping values and the measured values for these five specifications and identified the locations of maximum warping, as presented in TABLE 1 and TABLE 2. The results depicted in Fig. 7 to Fig. 11 and TABLE 1 and TABLE 2 indicate that the predicted C-warping distribution closely aligns with the actual measured values, with a maximum error not exceeding 15%, thus meeting the requirements of product accuracy.

The strip shape of the five specifications strip in each process section of CAF are predicted, and the causes of warping are analyzed, thereby providing theoretical guidance for the subsequent adjustment of the unit process parameters and

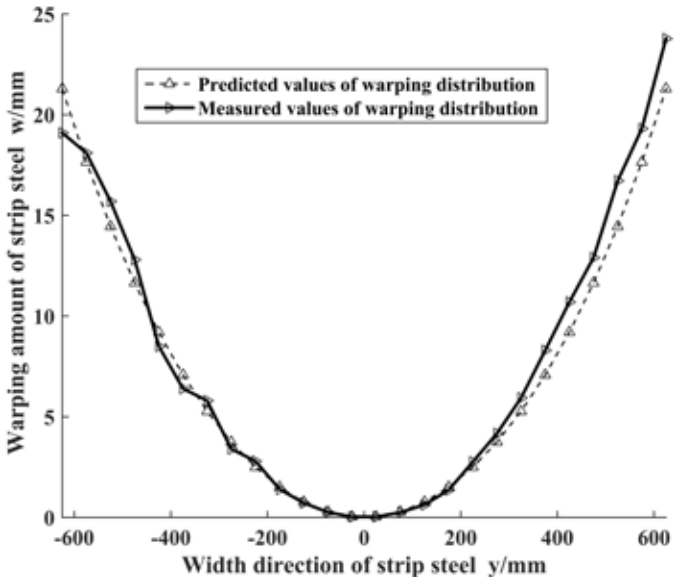

Fig. 7. Strip I warping distribution in unit outlet

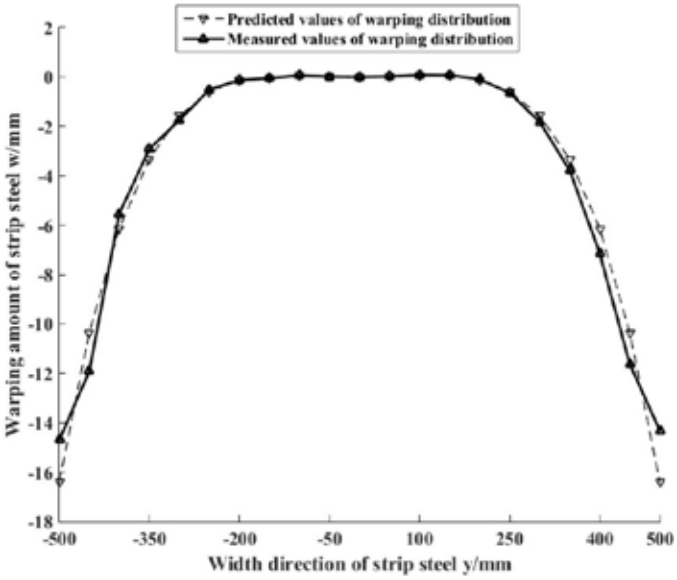

Fig. 8. Strip II warping distribution in unit outlet

TABLE 1

Comparison of Maximum C-Warping Values of Three Specifications of Exported Strip Steel by Line 208

C-warping defect index of strip	Strip I	StripII	Strip III
Predicted value of maximum warping/mm	21.3	−16.4	–4.47
Position of predicted value of maximum warping	Strip edge	Strip edge	Strip edge
Measured value of maximum warping /mm	23.8	−14.7	–4.67
Location of maximum warping	Transmission side of strip	Operation side of strip	Transmission side of strip
Relative error of maximum warping %	10.5%	11.5%	4.28%

TABLE 2

Comparison of Maximum C-Warping Values of Two Specifications of Exported Strip Steel by Line 108

C-warping defect index of strip	Strip IV	Strip V
Predicted value of maximum warping/mm	8.65	6.61
Position of predicted value of maximum warping	Strip edge	Strip edge
Measured value of maximum warping /mm	9.25	7.5
Location of maximum warping	Transmission side of strip	Operation side of strip
Relative error of maximum warping %	6.49%	11.89%

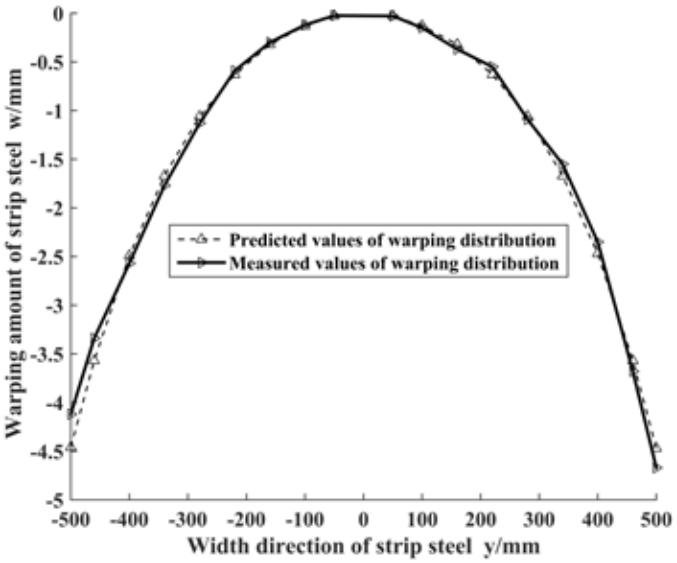

Fig. 9. Strip III warping distribution in unit outlet

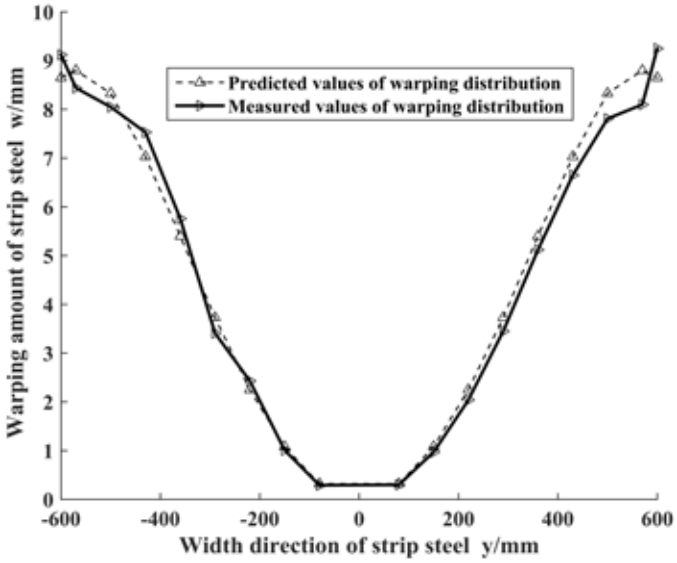

Fig. 10. Strip IV warping distribution in unit outlet

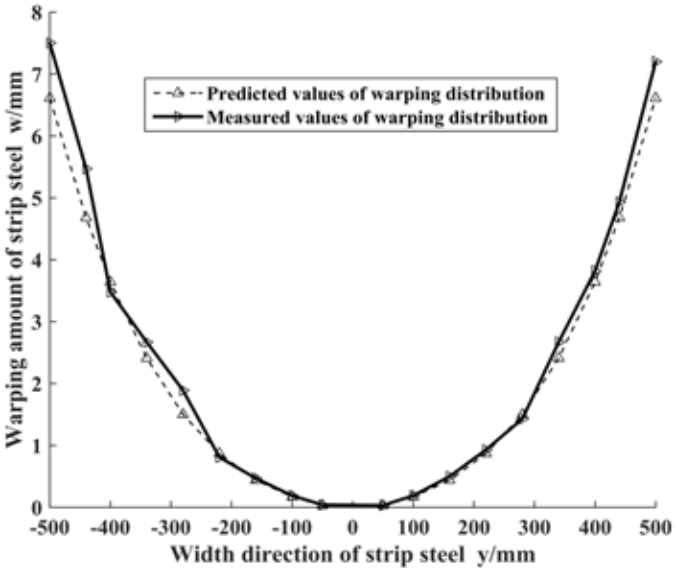

Fig. 11. Strip V warping distribution in unit outlet

decreasing incidence of C-warping defects. Strip shape evolution processes of the five specifications strip, are shown in Fig. 12 to Fig. 16, respectively.

In PHS, the temperature increase is modest. The five types of steel strips exhibit relatively flat shapes, with the maximum warping of I to V is 6.591, 10.55, 10.56, 3.51, 11.06 mm. In DFS, the flame of the heating device directly burn the strip surface. As the temperature rises sharply, a large elastic-plastic deformation is observed in all parts of the strip, and the warping on both sides increased sharply, with I to V reaching a maximum warping of 26.26, 15.41, –8.04, 38.24, and 32.01 mm. In RHS, the temperature difference at all parts of the strip surface are reduced, and part of the deformation are restored by radiation heating. The five specifications of strip have the similar trend, with I demonstrating a maximum warping of 19.8 mm, II at 15.41 mm, III at –2.06 mm, IV at 29.83 mm, and V at –14.74 mm.

In CS, significant differences arise in the process parameters for cooling the five types of steel strips. For Specification I, the cooling airflow does not effectively reduce the existing warping, instead exacerbating the degree of warping. The cooling fan parameters are not appropriately set to improve the C-warping. In contrast, for Specification II, IV, and V, the cooling airflow induces significant temperature drops, effectively compensating for the existing warpage in the opposite direction, resulting in a reverse warping phenomenon. Additionally, these strips maintain larger flat regions in the center, with reverse maximum warping of 16.4 mm, 8.65 mm, and 6.61 mm, respectively. For Specification III, the temperature drop in the CS section is minimal, leading to no significant temperature differences on the surface. Consequently, the warpage levels in the CS section do not markedly differ from those in RHS. This analysis illustrates that the rationality of the process parameter settings in the CS

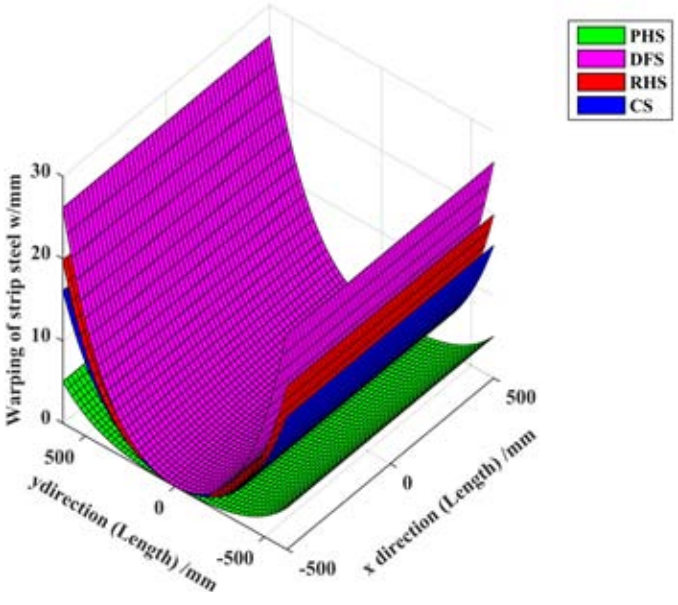

Fig. 12. Strip shape evolving of strip I

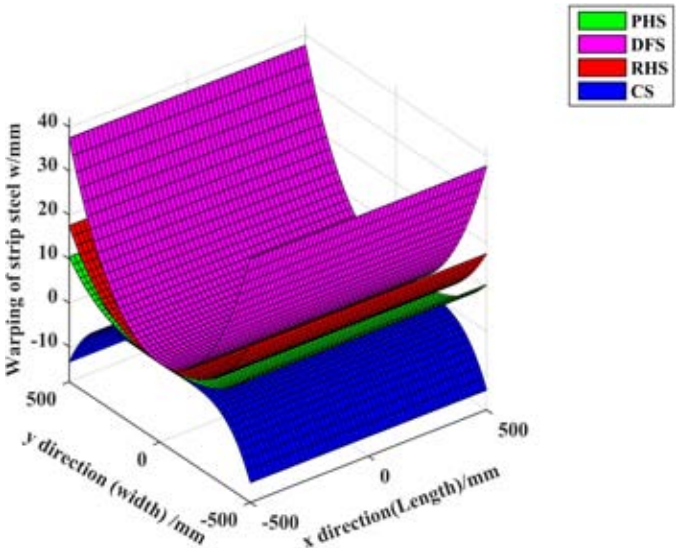

Fig. 13. Strip shape evolving of strip II

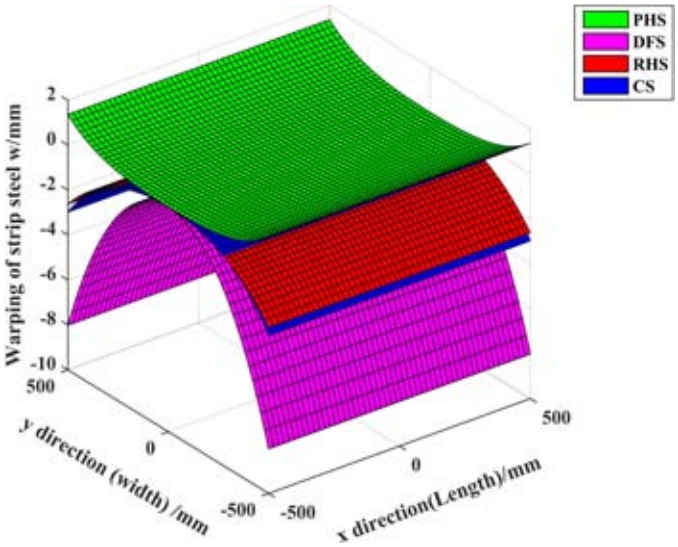

Fig. 14. Strip shape evolving of strip III

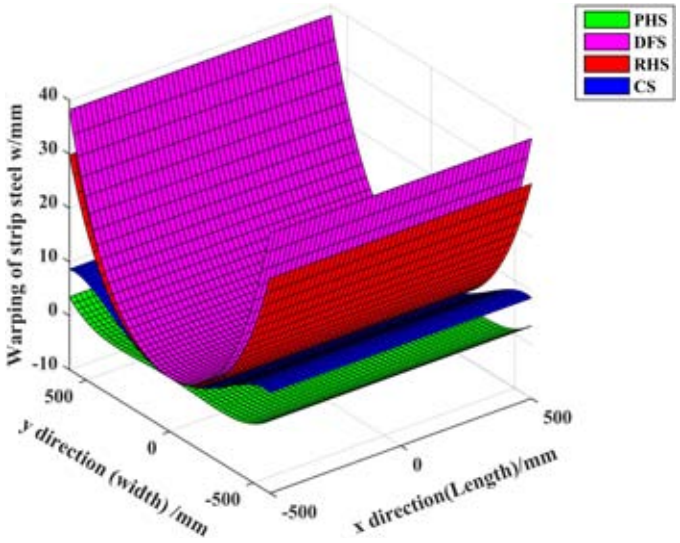

Fig. 15. Strip shape evolving of strip IV

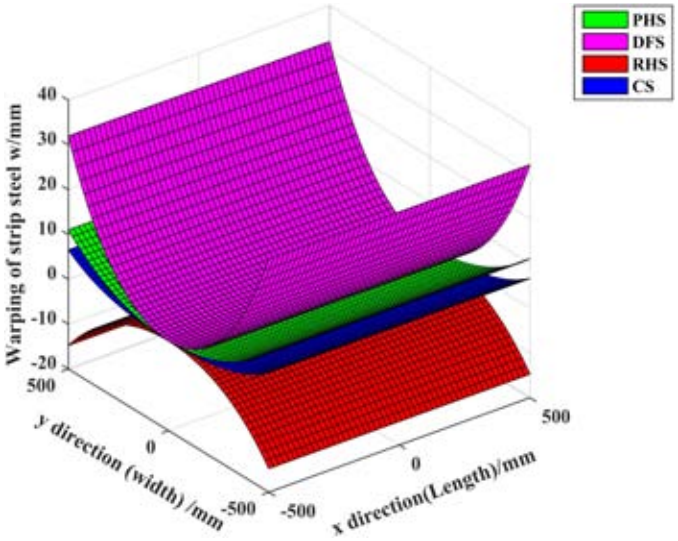

Fig. 16. Strip shape evolving of strip V

section not only directly influences the reverse compensation effect on warpage in the upstream process segments but also determines the effectiveness of improving the C-warping defects at the output of CAF.

5. Conclusion

(i) In CAP of HGU, the mechanical properties of the strip decreased nonlinearly with the temperature increasing. Based on elastoplastic theory, the C-warping mechanism was analyzed and C-warping defect mechanical model was derived by thermoelasticity theory and initial strain method. The essence of C-warping is that under high-temperature of CAF, the uneven distribution of strip surface temperature is resulting in the uneven transverse extension of the strip along thickness direction, which is caused by residual thermal stress.

(ii) The C-warping prediction model of the strip was established by strip element method on the basis of C-warping defect mechanical model, and an optimization recursive method was proposed to solve the problem that the strip surface temperature distribution along transverse direction cannot be obtained. The warping distribution of any transverse strip element can be calculated on the basis of C-warping defect mechanical model, which was represented by vector form.

(iii) The strip C-warping prediction model was applied on site. The C-warping calculation process was compiled according to the model, and the strip shape of five typical strips in CAP were calculated. The deviation between the measured value and the predicted value of the strip shape in the unit outlet are within error range of the product requirements. The model can predict the strip shape of process section in CAF and provide theoretical guidance for the optimization of the furnace process parameters.

Acknowledgements

A few experiments were made in Shanghai Meishan Iron and Steel Co., Ltd. We gratefully acknowledge the technical support of Shanghai Meishan Iron and Steel.

Funding

This work was supported by the University Natural Science Research Project of Anhui Province (2024AH051758), Key Scientific Research Funding Project of Huangshan University (2022xkjzd003), Research Start-up Project of Huangshan University (2024xkjq007, 2024xkjq001, 2024xkjq005), Horizontal Cooperation Funding Project of Huangshan University (hxkt2023214, hxkt2024214), Master Training Project of Huangshan University (hsxyssd008).

REFERENCES

[1] G. Nicolas, L. Catherine, S. Henri, Metall. Mater. Trans. B, **47**, 2666 (2016).
DOI: https://doi.org/10.1007/s11663-016-0672-3

[2] X.-L. Zan, F.-Q. Wang, Z.-Y. Liu, F. Li, China Metallurgy **30**, 35 (2020) (in Chinese).
DOI: https://doi.org/10.13228/j.boyuan.issn1006-9356.20190515

[3] X.-L. Zan, Y.-Z. Sun, F.-Q. Wang, F. Li, X.-D. Li, J. Wen, Steel Rolling **37**, 21 (2020) (in Chinese).
DOI: https://doi.org/10.13228/j.boyuan.issn1003-9996.20190110

[4] Q.-D. Zhang, J.-T. Dai, J. Univ. Sci. Technol. Beijing **33**, 1006 (2011) (in Chinese).
DOI: https://doi.org/10.13374/j.issn1001-053x.2011.08.014

[5] Q.-D. Zhang, X.-F. Lu, X.-F. Zhang, Engineering Mechanics **31**, 243 (2014) (in Chinese).

[6] J. Qin, Q.-D. Zhang, K.-F. Huang, Proc. 19th Annual National Conf. on Structural Engineering (ANCSE), (Jinan), The Chinese Society of Mechanics, Beijing 552 (2010).

[7] B.-Y. Zhang, X.-F. Lu, L.-Y. Zhang, Q.-D. Zhang, Chin. J. Mech. **54**, 184 (2018) (in Chinese).

[8] W. Tang, F.-S. Du, J. Wen, H.-H. Lin, Iron & Steel **54**, 55 (2019) (in Chinese).
DOI: https://doi.org/10.13228/j.boyuan.issn0449-749x.20190069

[9] J.-F. He, Baosteel Technology. **1**, 36 (2004) (in Chinese).

[10] B.-P. Zhang, L.-L. Zhou, China Metallurgy **6**, 55 (2007) (in Chinese).
DOI: https://doi.org/10.13228/j.boyuan.issn1006-9356.2007.07.006

[11] T. Masui, Y. Kaseda, K. Ando, ISIJ Int. **31**, 262 (1991).
DOI: https://doi.org/10.2355/isijinternational.31.262

[12] X.-F. Xu, Hot Dip Galvanizing Technology for Steel Strip, Chemical Industry Press, Beijing 19 (2007).

[13] R. Fang, MA. thesis, East China University of Science and Technology, (2017), https://kreader.cnki.net/Kreader/CatalogViewPage.aspx?dbCode=cdmd&filename=1018225687.nh&tablename=CMFD201802&compose=&first=1&uid=, (accessed 2017-12-17).

[14] GB51249-2017:2018, Code for fire safety of steel structures in buildings.

[15] X.-F. Lu, Ph.D. thesis, University of Science and Technology Beijing, (2015), https://kreader.cnki.net/Kreader/CatalogViewPage.aspx?dbCode=cdmd&filename=1015618082.nh&tablename=CDFDLAST2015&compose=&first=1&uid=, (accessed 2015-6-3).

[16] B.-Y. Xu, Elastoplastic mechanics and its applications, China Machine Press, Beijing 366 (1984).